This is a peer-reviewed, accepted author manuscript of the following research article: Yan, S., Shao, H., Min, Z., Peng, J., Cai, B., & Liu, B. (2023). FGDAE: a new machinery anomaly detection method towards complex operating conditions. Reliability Engineering and System Safety, 236, Article 109319. Advance online publication. https://doi.org/10.1016/j.ress.2023.109319

FGDAE: A new machinery anomaly detection method towards complex operating conditions

Shen Yan[1], Haidong Shao[1*], Zhishan Min[1], Jiangji Peng[1], Baoping Cai[2], Bin Liu[3]

1 College of Mechanical and Vehicle Engineering, Hunan University, Changsha 410082, China

2 College of Mechanical and Electronic Engineering, China University of Petroleum, Qingdao 266580 China

3 Department of Management Science, University of Strathclyde, Glasgow G1 1XQ, UK

Corresponding author: Haidong Shao (hdshao@hnu.edu.cn); Phone: +86 0731 88822330; Fax: +86 0731 88822330

Abstract: Recent studies on machinery anomaly detection only based on normal data training models have yielded good results in improving operation reliability. However, most of the studies have problems such as limiting the detection task to a single operating condition and inadequate utilization of multi-channel information. To overcome the above deficiencies, this paper proposes a new machinery anomaly detection method called full graph dynamic autoencoder (FGDAE) towards complex operating conditions. First, a full connected graph (FCG) is developed to obtain the global structure information by establishing structural connections between every two channels. Subsequently, a graph adaptive autoencoder (GAAE) model is constructed to aggregate multi-perspective feature information between channels by adapting changes of the operating conditions and to reconstruct the information containing the essential features of normal data. Finally, a dynamic weight optimization (DWO) strategy is designed to guide the model learning the generalization features by flexibly adjusting the data reconstruction loss weights in each condition. The proposed method performs multi-condition anomaly detection under the challenge of training models with multi-condition unbalanced normal data and achieves better performance compared to other popular anomaly detection methods on the machinery datasets.

Keywords: Machinery anomaly detection; Complex operating conditions; Multiple channels; Full graph dynamic autoencoder; Weight optimization strategy; Graph convolution network.

1. Introduction

Health monitoring of machinery plays an essential role in sustaining industrial reliability due to the wide use of machinery in various industries [1-3]. With the widespread use of sensors, machinery generates a large amount of data during operation, and how to effectively perform health monitoring

based on the data has become a hot research topic in recent years [4-6].

Deep learning has become one of the mainstays for data-driven health monitoring with its simplicity in reducing domain experience [7], including convolutional neural network (CNN) [8, 9], long short-term memory (LSTM) [10, 11], autoencoders [12, 13], generative adversarial network (GAN) [14, 15] and so on. Sparse deep learning has been applied to identify machinery defection at constant [16] and varying speed [17, 18], which is putting the constraint on the activation of neurons. In the past three years, machinery anomaly detection only based on normal data to train model has gained increasing attention. Dai *et al.* [19] proposed an anomaly detection method for mechanical health monitoring using the advantages of autoencoder and GAN. Plakias *et al.* [20] achieved anomaly detection of machinery by integrating different types of autoencoders. Chen *et al.* [21] constructed a new deep residual shrinkage relation network to detect the anomaly state of rotating machinery. The above anomaly detection methods relax the requirement for faulty samples to some extent, but they are all performed with a single sensor channel and ignore the rich feature information contained in multi-channel data. In 2022, Yan *et al.* [22] introduced a memory-augmented skip-connected autoencoder for anomaly detection of rocket engines with multi-channel data. In the same year, Yan *et al.* [23] suggested a robust convolutional autoencoder that exploits multi-channel information under noise to achieve anomaly detection of machine tools. They preliminarily explore the multi-channel information, but fail to mine the structural information between different channel data.

Non-Euclidean graph (NEG) can establish structural connections between data, and further aggregate information of neighbor nodes through graph convolution network (GCN), which has been increasingly studied for health monitoring of machinery in the last two years. The NEGs can be broadly classified into two categories according to the method of constructing graphs: graph level and node level [24]. Graph-level NEGs can establish connections within the single sample, with one NEG representing one sample. Li *et al.* [25] framed the sensor network graph for each sample and mined spatial-temporal information by attentional GCN and LSTM for residual life prediction. Tang *et al.* [26] transformed a vibration sample into a symmetric snowflake image to identify motor states in transients by cardinality preserving graph attention network (GAT). Li *et al.* [27] constructed a sample into a weighted horizontal visibility graph and implemented fault diagnosis of bearings by GCN. Instead, node-level NEGs can establish connections between different samples, with multiple samples forming a NEG. Zhao *et al.* [28] designed an adaptive local graph learning method by constructing inter-sample

connections to achieve semi-supervised fault diagnosis of motor-bearing system. Yang *et al.* [29] introduced the k-nearest neighbor (KNN) algorithm and GCN to aggregate information between different samples for cross-domain machinery fault diagnosis. Yan *et al.* [30] designed a label propagation strategy for node-level graphs based on KNN algorithm and implemented semi-supervised machinery fault diagnosis by dynamic GAT.

The above graph structure methods can mine the structural information among data, but their model training all relies on faulty samples, which reduces the feasibility of the methods. Moreover, the existing studies on machinery anomaly detection are often limiting the detection task to a single operating condition. In the engineering practice, the operating conditions of machinery often change with different requirements, with significant differences in the number and distribution features of normal data under each operating condition. Therefore, it is valuable to study graph structure methods to aggregate information of muti-channels for machinery multi-condition anomaly detection under the challenge of training models with multi-condition unbalanced normal data.

This study proposes a novel FGDAE, which can effectively aggregate multi-perspective feature information between channels and perform anomaly detection towards complex operating conditions. The main innovations can be summarized in the following four aspects. (1) The FCG is developed to obtain the global structure information by establishing structural connections between every two channels. (2) The GAAE model is constructed to aggregate multi-perspective feature information between channels by adapting changes of the operating conditions and to reconstruct the information containing the essential features of normal data. (3) The DWO strategy is designed to guide the model learning the generalization features by flexibly adjusting the data reconstruction loss weights in each condition. (4) The new graph structure method is proposed for machinery multi-condition anomaly detection under the challenge of training models with multi-condition unbalanced normal data.

This paper is organized as follows: Section 2 introduces the related theories. Section 3 presents the proposed method, which includes the elaboration of three modules and overall steps of the proposed method. Section 4 provides a comprehensive experiment validation. Section 5 gives the conclusion of the paper.

2. Related theories

2.1. Spectral GCN

The spectral CNN proposed by Bruna *et al.* [31] is considered as the prototype of spectral GCN,

which extends the convolution from Euclidean space to irregular non-Euclidean graph data. It can be briefly expressed as below:

$$Z = \sigma\left(UgU^T X\right) \tag{1}$$

where X is the input data; Z is the output data; g is the graph convolution kernel; σ is the nonlinear activation function; U represents the Laplacian eigenvector of the graph, where U^T is used for the graph Fourier transform of X and U is for the graph inverse Fourier transform. U is obtained by the Laplacian matrix eigen-decomposition, which can be expressed as follows:

$$L = U\Lambda U^T \tag{2}$$

where L is the graph Laplacian matrix; Λ is the graph Laplacian eigenvalue matrix. Since the spectral CNN explicitly uses Laplacian matrix eigen-decomposition, it leads to large computational cost and non-localization of the convolution kernel. Defferrard *et al.* [32] parameterizes the convolution kernel g by polynomial approximation, which can be expressed as follows:

$$g = \sum_{k=0}^{K-1} \theta_k \Lambda^k \tag{3}$$

where θ are the learned model parameters; K is the hyperparameter, indicating the Chebyshev filter size. Then Eq. (1) can be expressed as follows:

$$Z = \sigma\left(U\sum_{k=0}^{K-1}\theta_k\Lambda^k U^T X\right) = \sigma\left(\sum_{k=0}^{K-1}\theta_k L^k X\right) \tag{4}$$

where $L^0 = I$; I is the unit matrix. Eq. (4) eliminates U well, thus avoiding the Laplacian matrix eigen-decomposition.

2.2. Denoising autoencoder

To overcome the limitation of the traditional autoencoder that has the risk of overfitting when reconstructing data features, Vincent *et al.* [33] proposed the denoising autoencoder (DAE). Its core idea is to learn the robust features by adding random noise into the input data, which can be briefly expressed as follows:

$$X' = X + \text{Noise} \tag{5}$$

where Noise is the added random noise and X' is the input data with noise. Then, the reconstruction loss can be expressed as follows:

$$\text{Loss} = (X'' - X)^2 \tag{6}$$

where X'' is the reconstructed data; Loss represents the reconstruction loss. In summary, the structure

of the DAE can be shown in Fig. 1.

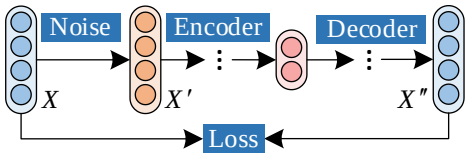

Fig.1. The structure of the DAE.

3. The proposed method

This study proposes the FGDAE for machinery multi-condition anomaly detection under the challenge of training models with multi-condition unbalanced normal data, which consists of three parts: development of the FCG, construction of the GAAE model and design of the DWO strategy.

3.1. Development of the FCG

Although some of existing studies for anomaly detection use multi-channel data, they all ignore the structural information between different channels. Therefore, the study develops the FCG to overcome the above deficiency, described as below.

The FCG is a concise graph-level NEG, where one graph represents a sample under one operating condition. The structural connections between every two channels can be established by creating edges between every two nodes, which can be expressed as follows:

$$A_{ij} = \left[X^i, X^j \right] = 1 \quad \left(i \neq j,\ i, j = 1, 2 \cdots N \right) \tag{7}$$

where N represents the number of sensor channels; X^i is the original data of the i-th channel; $[\cdot]$ represents the operation of constructing graph; A_{ij} is the i-th row and j-th column value of the graph adjacency matrix, which can be used to calculate the graph Laplacian matrix L. It can be expressed as below:

$$L = D - A \tag{8}$$

$$D_{ii} = \sum_{j=1}^{N} A_{ij} \tag{9}$$

where D is the degree matrix of the graph that is the diagonal matrix. For the simplicity and beauty of the presentation, the FCG of fusing 4-channel information can be visually presented as Fig.2, which can be interpreted as a global connection between channel data. It should be reminded that two experimental cases are FCGs of fusing 6 channels and fusing 8 channels respectively, but the construction principles are the same as the Fig.2.

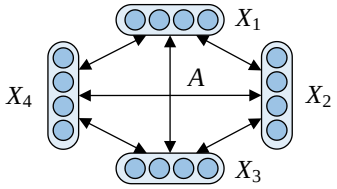

Fig.2. The FCG of fusing 4-channel information.

3.2. Construction of the GAAE model

Existing anomaly detection models fail to aggregate multi-perspective feature information between sensor channels, and the general DAE cannot adapt changes of the operating conditions. This study constructs the GAAE model to overcome the above limitations.

After obtaining the graph data constructed by FCG, adaptive Gaussian noise is added to the data, which can be expressed as follows:

$$X' = X + C \times \bar{X} \times N(0,1) \tag{10}$$

where $N(0,1)$ represents Gaussian noise of standard normal distribution; $\bar{X}$ is the average value of the input data X; C represents the number of operating conditions within the input data. As the number of conditions increases, the noise level will increase as well, which can further reduce the domain distribution differences of the data in different conditions.

Then the graph data containing adaptive noise is fed into the GCN with the autoencoder structure. Unlike the variational graph autoencoder [34] reconstructing graph structure, the constructed GAAE model is reconstructed from the perspective of node features. Multi-perspective feature information between channels is aggregated by GCN, and the information containing the essential features of normal data is reconstructed with the autoencoder structure. The visualization of the GAAE model is shown in Fig. 3, where the graph convolution encoder and graph convolution decoder can be expressed by the following equations.

$$H = \sigma\left(W\left(\sum_{k=0}^{K-1}\theta_k L^k X'\right) + b\right) \tag{11}$$

$$X'' = \sigma\left(W'\left(\sum_{k=0}^{K-1}\theta'_k L^k H\right) + b'\right) \tag{12}$$

where W and b are the weight parameter and bias parameter of the linear transform in the graph convolution encoder, which is used for the compression of high-dimensional features; θ is the learned parameter of the GCN in the encoder; H is the compressed graph data after encoder; W' and b' are the weight parameter and bias parameter of the linear transform in the graph convolution decoder, which is

used for the reconstruction of the feature dimension.; θ' is the learned parameter of the GCN in the decoder; X'' is the reconstructed graph data after decoder; σ is chosen as the ReLU activation function. The structural parameters of the GAAE model are listed in Table 1.

It is important to note that there are multiple operating conditions with normal graph data fed into the model training at the same time. In order to subsequent application of the DWO strategy, the reconstruction loss of the normal data under each operating condition needs to be calculated separately, which can be expressed as follows.

$$\text{Loss}_l = (X_l'' - X_l)^2 \ (l = 1, 2, \cdots, C) \tag{13}$$

where Loss_l is the reconstruction loss of the l-th operating condition; X_l is the input data of the l-th operating condition; X_l'' is the output data of the l-th operating condition.

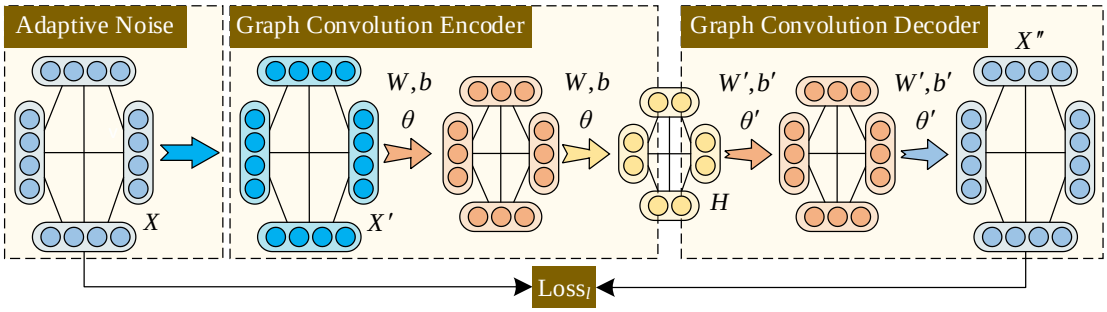

Fig.3. The structure of the GAAE model.

Table 1

The structural parameters of the GAAE model.

Layer	GCN (K=2)	Linear transform	Input/output size	Batch normalization	Activation function
Encoder1	Yes	Yes	512/64	Yes	ReLU
Encoder2	Yes	Yes	64/16	No	\
Decoder1	Yes	Yes	16/64	Yes	ReLU
Decoder2	Yes	Yes	64/512	No	\

3.3. Design of the DWO strategy

Most of the studies on machinery anomaly detection are limiting the testing task to a single operating condition, and the model training does not consider the interference of multi-condition unbalanced normal data. Therefore, the study designs the DWO strategy for this challenging scenario.

When the training data is unbalanced between different operating conditions, the model tends to

ignore the feature information of the condition with less data, leading to the larger reconstruction loss. Inspired by applying dynamic weight averaging for multi-task learning in [35], the study designs the DWO strategy to flexibly adjust the data reconstruction loss weight under each condition, which can be expressed as follows:

$$r_l^t = C \times \frac{\text{Loss}_l^t}{\text{Loss}_l^{t-1}} \tag{14}$$

$$w_l^t = \frac{\exp(r_l^t)}{\sum_{l=1}^{C} \exp(r_l^t)} \tag{15}$$

$$\text{Loss}^t = w_1^t \text{Loss}_1^t + \cdots + w_l^t \text{Loss}_l^t + \cdots + w_C^t \text{Loss}_C^t \tag{16}$$

where t represents the number of iterations; Loss^t represents the total reconstruction loss in t-th iteration; r_l^t is the training speed in t-th iteration under the l-th condition, and its smaller value means faster speed; when $t = 0$, r_l^0 is 1; w_l^t is the weight of the data reconstruction loss in t-th iteration under the l-th condition, which can be dynamically optimized based on r_l^t in each iteration. According to Eqs.(14-16), it can be easily found that if r_l^t is smaller, w_l^t will also be smaller, which can effectively balance the training speed of the GAAE model under each condition in order to guide the model learning the generalization features.

Finally, the loss value obtained from Eq.(16) is back propagated through the Adam optimizer [36] to optimize the model parameters.

3.4. Overall steps of the proposed method

The overall steps of the FGDAE are shown in Fig.4 and elaborated below.

Step 1: The multi-channel unbalanced data under multi-conditions (MCUD-MC) is acquired from the experimental bench and constructed as the graph data based on Eq.(7) of the FCG. The graph data is then divided into the training set only containing unbalanced normal graph data under multi-conditions and the test set containing both normal and faulty graph data under multi-conditions.

Step 2: Set the model hyperparameters and randomly initialize the learning parameters. Adaptive noise based on Eq.(10) is added to the training set, and then fed into the constructed GAAE model to aggregate multi-perspective feature information between channels. The reconstructed graph data is obtained based on Eqs.(11, 12), and then the reconstruction loss of the graph data under each condition is calculated by Eq.(13). Finally, the total loss value is calculated by Eqs.(14-16) of the DWO strategy,

and the learning parameters are updated iteratively by the Adam optimizer.

Step 3: Input the training set data without adaptive noise into the trained model to calculate the loss values of all normal graph data. In order to demonstrate the feature learning ability of the model, the maximum value is determined as the threshold for detecting faulty data, `which effectively avoids the manual adjustment of the threshold and the difficulty of percentage interval selection.

Step 4: The muti-condition test set without adaptive noise is imported into the trained model, and the loss value is counted for every test sample to determine the normal or fault based on the threshold value. Finally, anomaly detection results are obtained by calculating the evaluation metrics.

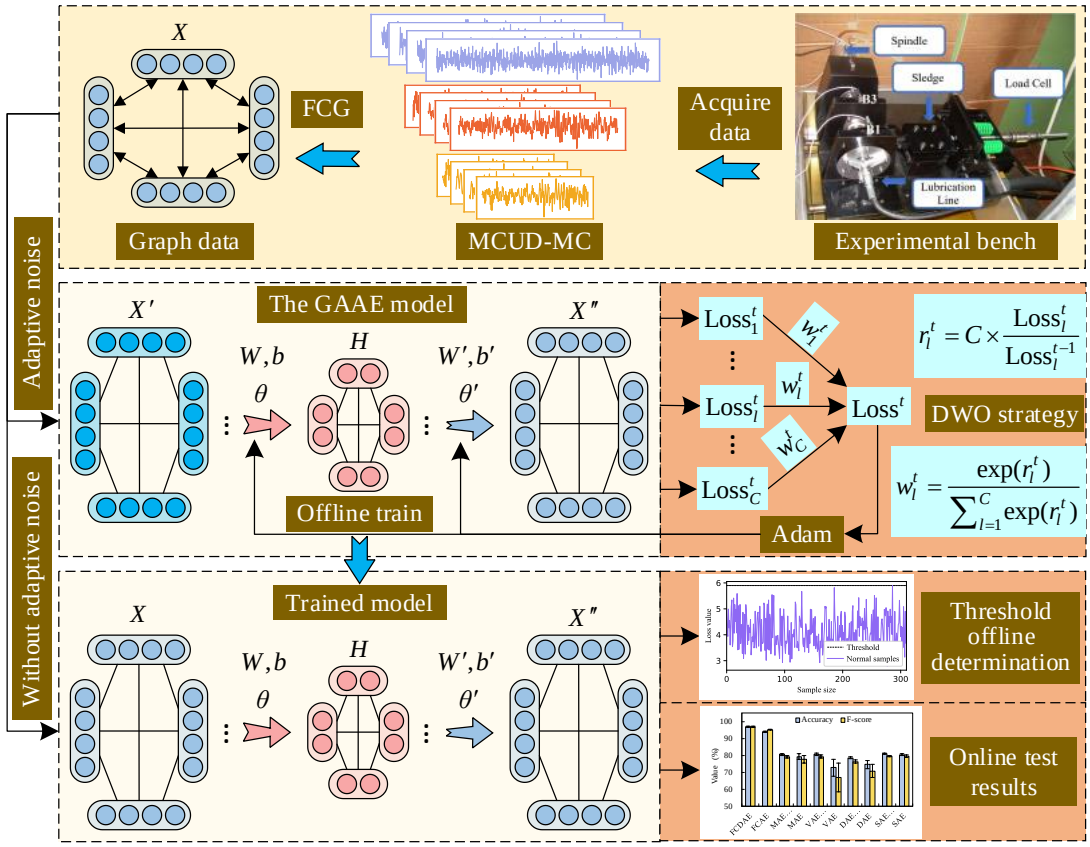

Fig.4. Overall steps of the FGDAE.

4. Validation of experiments

4.1. Introduction to the datasets

The superiority of the proposed method for muti-condition anomaly detection under the challenge of training models with multi-condition unbalanced normal data is validated on two machinery cases.

Case 1: The dataset is derived from the high-speed aerospace bearings of the Politecnico di Torino [37], and the experimental setup is shown in Fig. 5. B1, B2, and B3 are three bearings; two triaxial acceleration sensors are installed at A1 and A2 to measure the vibration data of six channels

simultaneously; Table 2 lists the acceleration direction of each channel. The operating conditions are changed by varying the speed and load of the bearings. In each condition, data is collected for the normal state and six different levels of fault states with sampling frequency of 51,200Hz.

Case 2: The dataset is derived from the gearbox of the Southeast University [38], with the experimental bench shown in Fig. 6 (a). There are 8 sensor channels measuring the torque and vibration of the motor, the *x*, *y* and z vibration of the planetary gearbox and the parallel gearbox, respectively, with sampling frequency of 5 kHz [39]. The conditions depend on the speed and load of the gearbox; the normal state and four gear fault states are measured for each condition, as shown in Fig. 6 (b).

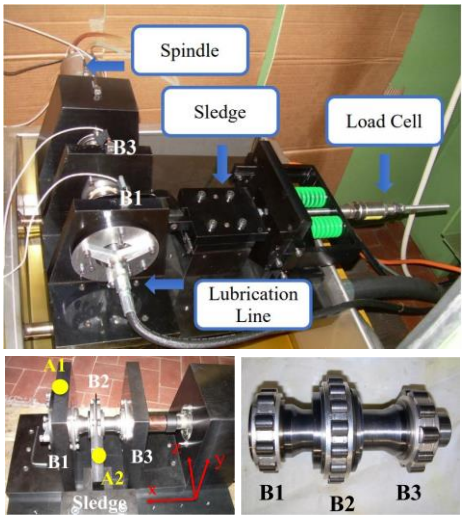

Fig.5. Experimental setup of Case 1.

Table 2

Acceleration direction of each channel in Case 1.

Sensors	A1			A2		
Channels	Channel 1	Channel 2	Channel 3	Channel 4	Channel 5	Channel 6
Direction	*x*-axial	*y*-radial	*z*-radial	*x*-axial	*y*-radial	*z*-radial

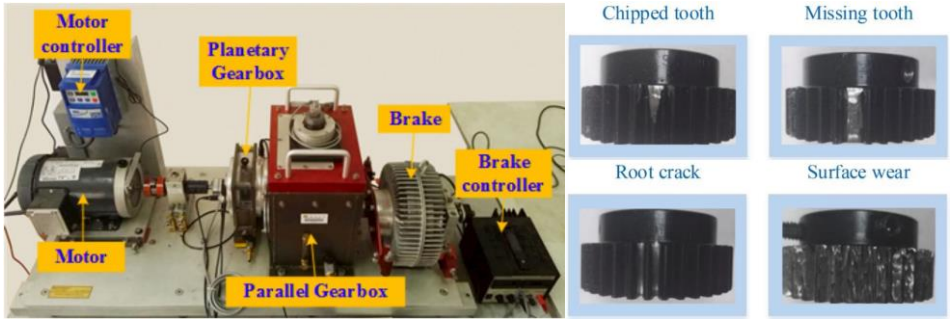

(a) (b)

Fig.6. Experimental setup of Case 2: (a) The experimental bench; (b) Fault Type.

In this paper, the samples used in both cases are described in Table 3. It should be noted that the

multi-condition unbalance is for the normal samples in the training set, and there is no faulty sample in the training set; the test set contains both normal and faulty samples for multi-conditions. Case 1 contains three different high-speed conditions and Case 2 contains two different lower-speed conditions, all of them with different speeds and loads. The maximum unbalanced ratio of normal samples in the training set between the conditions is up to 20 times (200/10) for both cases. In order to fully demonstrate the anomaly detection performance of each method, 50 samples for every fault type are randomly collected in the test set under each condition. Since there are 6 fault types in Case 1, the total number of faulty samples is 300 under each condition; Case 2 has 4 fault types, the total number of faulty samples is 200 under each condition. In addition, the normal samples are 200 in the test set under each condition. There are three conditions in Case 1, so the total number of samples in the test set is 1500; Case 2 has two conditions, thus the total number of samples in the test set is 800. The training process is to feed all the training samples in Case 1 or Case 2 into the model; the testing process is to feed all the test samples in the corresponding Case into the model to complete the detection.

Table 3

Description of the data used in both cases.

Cases	Conditions	Health states	Training samples	Test samples
Case 1	200Hz, 0N	Normal	200	200
		Fault	\	300
	300Hz, 1000N	Normal	100	200
		Fault	\	300
	400Hz, 1400N	Normal	10	200
		Fault	\	300
Case 2	20Hz, 0V	Normal	200	200
		Fault	\	200
	30Hz, 2V	Normal	10	200
		Fault	\	200

Fig. 7 visualizes the normal data of the six sensor channels for the three conditions in Case 1, and the six groups of signals from top to bottom correspond to the six channels in Table 2. It can be intuitively observed that the signal characteristics are different among the sensor channels, which record the data information under the corresponding channels respectively, so it is necessary to

aggregate multi-perspective feature information between them. In addition, although they are all normal data, the vibration data between the three conditions have a large difference, and the vibration amplitude is even several multiples different. Therefore, it is challenging to learn the generalization features under the multi-condition unbalanced normal data training model.

In the experiments, all methods are repeated five times in order to reduce the effect of the randomness. Based on experience and the idea of greedy algorithm [40], the main hyperparameters are set as follows: the batch size is 64; the number of iterations is 200; the initial value of learning rate is 0.01, which decays by 0.1 times at 10 and 100 iterations, respectively. The running configuration is described as follows: the software is Pytorch 1.7.1; GPU is GTX1650; CPU is i5-10400F.

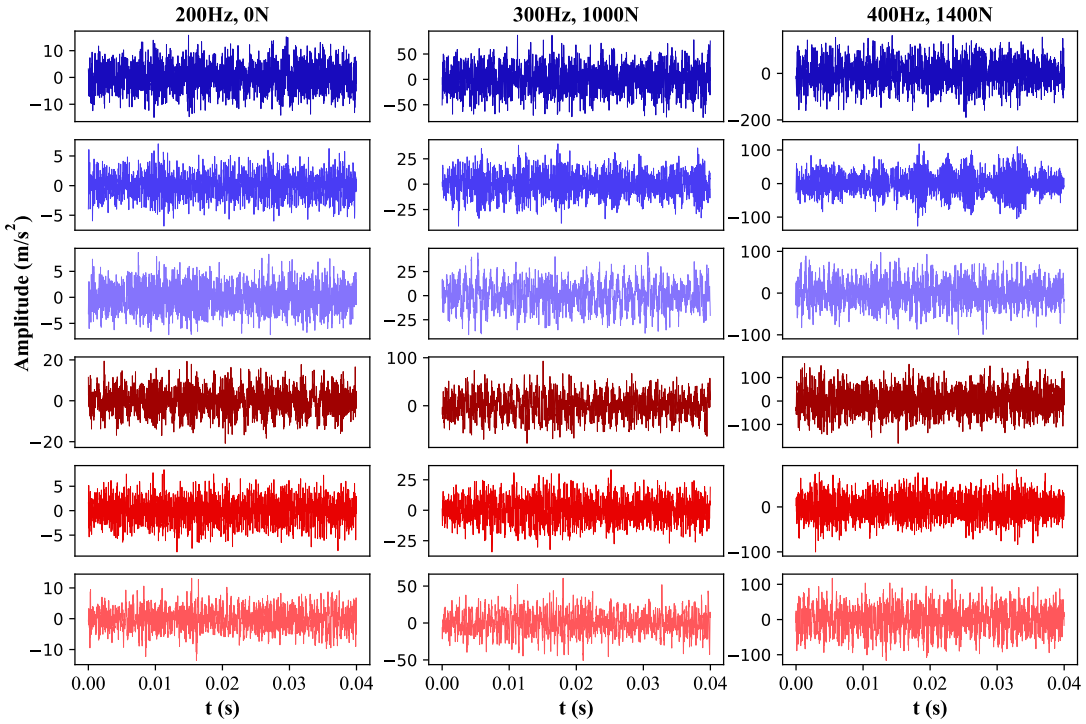

Fig.7. Multi-channel normal data for the three conditions in Case 1.

4.2. Superiority of the proposed method

In this subsection, we verify the superiority of the proposed FGDAE for anomaly detection towards complex operating conditions and compare it with the popular anomaly detection methods, including memory-augmented autoencoder (MAE) [41], variational autoencoder (VAE) [42], DAE [34] and SAE [43]. The anomaly detection evaluation metrics involved are calculated as follows:

$$\text{Accuracy} = (TP + TN) / (TP + TN + FP + FN) \tag{17}$$

$$\text{Precision} = TP / (TP + FP) \tag{18}$$

$$\text{Recall} = TP / (TP + FN) \tag{19}$$

$$\text{F-score} = 2 \times (\text{Precision} \times \text{Recall}) / (\text{Precision} + \text{Recall}) \quad (20)$$

where TP indicates correctly detected as faulty samples; TN indicates correctly detected as normal samples; FP means error detection as faulty samples; FN means error detection as normal samples.

Table 4 shows the evaluation metrics and running times of each method in Case 1. Four evaluation metrics of the proposed method reach 94.64%, 92.28%, 99.53%, and 95.74%, respectively, which are better than the comparison methods and fluctuate in a reasonable range. The anomaly detection result of the MAE is second only to the proposed method, but all the metrics are still lower than the proposed method by 8.77%, 3.01%, 13.88%, and 8.34%, respectively. Although the offline training time of the proposed method is relatively high, its online time is the shortest, with only 0.9 s for 1500 test samples.

Table 4

Evaluation metrics and times of each method in Case 1.

Unsupervised methods	Evaluation metrics (%)				Times (s)	
	Accuracy	Precision	Recall	F-score	Offline	Online
FGDAE	**94.64±2.14**	**92.28±3.53**	**99.53±0.71**	**95.74±1.62**	38	0.9
MAE	85.87±1.19	89.27±0.37	85.65±2.59	87.40±1.24	14	1.1
VAE	82.68±2.78	88.46±2.04	80.42±6.94	84.07±3.34	15	1.1
DAE	80.27±2.28	89.26±0.27	74.56±4.54	81.19±2.68	15	1.1
SAE	85.29±1.83	88.75±0.54	85.16±3.90	86.87±1.95	47	1.1

Table 5 shows the evaluation metrics and running times of each method in Case 2. The proposed method achieves 96.95%, 98.60%, 95.25%, 96.90% for all evaluation metrics, respectively, which is much better than the comparison methods and has the best stability. In Case 2, the SAE achieves the second best result, but all the metrics are still 16.5%, 24.88%, 8.89%, and 17.36% lower than the proposed method, respectively. The proposed method also has the shortest online testing time, with only 0.5 s for 800 test samples. Meanwhile, we visualize the loss values of each method for all test samples in Case 2, as shown in Fig. 8. It should be noted that the threshold of each method is adaptively determined according to step 3 in section 3.4. Specifically, the maximum reconstruction loss value of 210 training samples under two conditions in Case 2 is taken as the threshold. The horizontal coordinate is the sample size; the first 200 samples are normal samples and the last 200 samples are faulty samples; the red and blue lines represent the two different conditions, respectively. The normal sample curves of the proposed method are highly overlapping under the two conditions, indicating that

the loss values are similar, and the distinction between normal and faulty samples is significant. It is proved that the proposed method can learn the generalization features towards complex conditions. However, the four comparison methods prefer to ignore the data features under the fewer training samples' condition, so the reconstruction loss value will be higher, as shown as the red curves of normal samples being higher than blue curves.

Table 5

Evaluation metrics and times of each method in Case 2.

Unsupervised methods	Evaluation metrics (%)				Times (s)	
	Accuracy	Precision	Recall	F-score	Off-line	Online
FGDAE	**96.95±0.40**	**98.60±0.35**	**95.25±0.66**	**96.90±0.41**	29	0.5
MAE	79.27±1.61	73.62±0.75	82.39±4.35	77.73±2.32	10	0.7
VAE	72.78±4.99	70.65±2.17	64.54±14.53	66.96±8.59	11	0.7
DAE	74.57±2.35	71.30±1.18	70.51±6.34	70.82±3.79	11	0.7
SAE	80.45±0.61	73.72±0.54	86.36±1.42	79.54±0.74	31	0.7

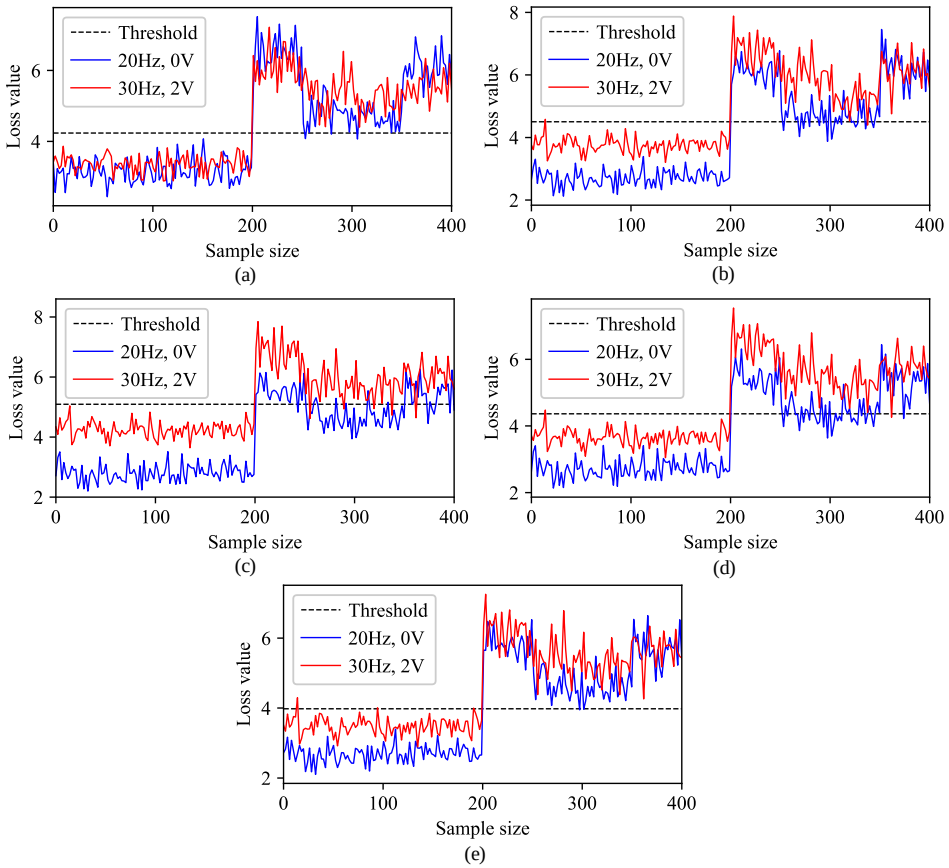

Fig.8. The loss values of the methods in Case 2: (a) FGDAE; (b) MAE; (c) VAE; (d) DAE; (e) SAE.

4.3. Validity of each module

In this subsection, we verify the validity of the FCG, adaptive Gaussian noise in Eq.(10), and the DWO strategy, respectively.

First, we demonstrate the validity of the FCG and adaptive Gaussian noise towards complex operating conditions, comparing them with the commonly used KNN graph construction [29, 30] based on Euclidean distance measurement and ordinary Gaussian noise respectively. The number of neighbor nodes in KNN is 3, which can be understood as the local similar connection between channel data. Fig. 9 shows the confusion matrices for the three methods in Case 1, where GDAE represents the graph denoising autoencoder (with the addition of ordinary Gaussian noise). In here, the horizontal coordinates are the true labels and the vertical coordinates are the predicted labels, where coordinates 0, 2, and 4 are the normal samples under the three conditions in Table 3; coordinates 1, 3, and 5 are the corresponding faulty samples. For the first condition with 200 training samples, all three methods show good anomaly detection results. In the second condition with 100 training samples, i.e. the yellow box, the KNN graph construction starts to perform worse compared to the developed FCG, because the FCG establishes global connection between channel data to guide model better obtaining multi-perspective feature information. In the third condition with only 10 training samples, i.e. the red box, although all the faulty samples are detected by FCG+GDAE+DWO, more than half of the normal samples are falsely detected as faulty samples. It reflects that the GDAE tends to fit the data features under other two conditions and fails to learn the data features under this condition well.

Fig. 10 shows the 2D visualization of encoded features for the three methods in Case 2, where Normal 1 and Normal 2 represent the normal samples of the two conditions in Table 3, respectively; Fault 1 and Fault 2 are the corresponding faulty samples. The proposed method has the most significant degree of differentiation between normal and faulty samples for both conditions, while KNN and GDAE have partial overlap between normal and faulty sample features under the condition with only 10 training samples. The results are consistent with those shown in Fig. 9.

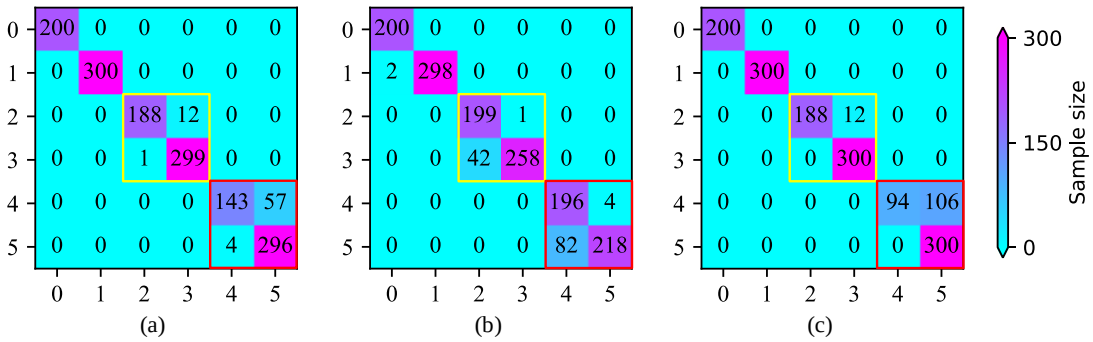

Fig.9. Confusion matrices for the three methods in Case 1: (a) FCG+GAAE+DWO (The proposed method); (b) KNN+GAAE+DWO; (c) FCG+GDAE+DWO.

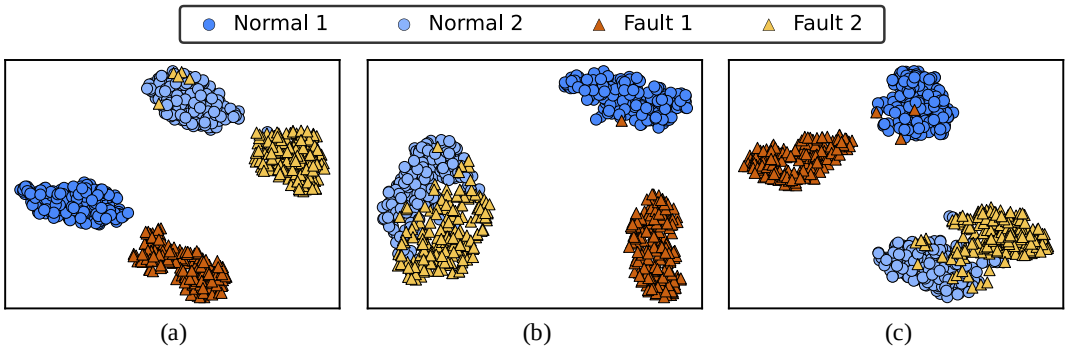

Fig.10. 2D visualization of encoded features for the three methods in Case 2: (a) FCG+GAAE+DWO (The proposed method); (b) KNN+GAAE+DWO; (c) FCG+GDAE+DWO.

Then, we demonstrate the validity of the DWO strategy towards complex operating conditions, by comparing the methods in Table 4 with or without adding the DWO strategy. Fig. 11 shows the accuracy and F-score of each method for anomaly detection, where FGAE represents FCG+GAAE without the DWO strategy. In Case 1, by adding the DWO strategy, the accuracy and F-score of FGAE is improved by 0.49% and 0.46%, respectively; MAE is improved by 2.37% and 2.42%; VAE is improved by 7.63% and 7.83%; DAE is improved by 9.6% and 10.32%; SAE is improved by 4.46% and 5.61%. Similarly in Case 2, the accuracy and F-score of FGAE is improved by 2.80% and 1.62%, respectively; MAE is improved by 1.25% and 1.40%; VAE is improved by 7.92% and 12.35%; DAE is improved by 3.95% and 5.57%; SAE is improved by 0.58% and 0.17% by adding the DWO strategy. In both cases, almost all methods show some reduction in volatility with the addition of the DWO strategy. This is because the DWO strategy can guide the model learning the generalization features between conditions by flexibly adjusting the data reconstruction loss weights in each condition.

To further explore the efficacy of the DWO strategy for anomaly detection in each condition, we plot the confusion matrices of some methods in Case 2, as shown in Fig. 12. The meanings of the

coordinate axes are the same as Fig. 9; coordinates 0, 2 are the normal samples under the two operating conditions in Case2; coordinates 1, 3 are the corresponding faulty samples. The FGAE performs badly for anomaly detection under the condition with only 10 training samples, as a large number of normal samples are falsely detected as faulty samples. It is because FGAE fails to learn the data features of this condition well, so that the loss values of normal samples in the test set of this condition are relatively high. Similarly, the DAE performs worse for anomaly detection with 200 training samples, as a lot of faulty samples are undetected. It is also because the DAE fails to learn the data features of the few-sample condition well, resulting in a high threshold for detecting faulty samples.

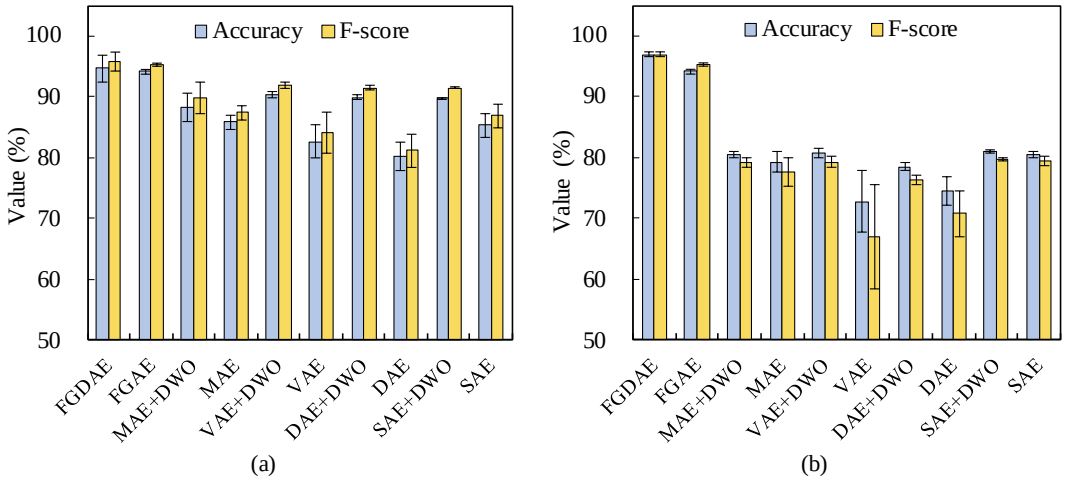

Fig.11. Evaluation metrics for the methods: (a) Case 1; (b) Case 2.

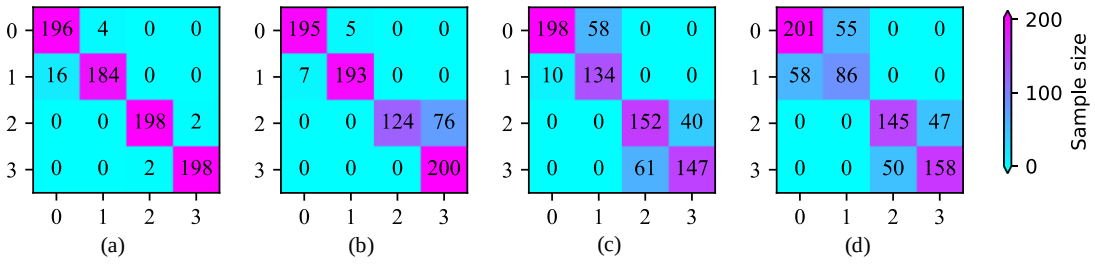

Fig.12. Confusion matrices for the four methods in Case 2: (a) FGDAE; (b) FGAE; (c) DAE+DWO; (d) DAE.

4.4. Discussion of the single condition data

Finally, we discuss the anomaly detection results of each method in Table 4 under the single condition with different numbers of training samples. Since the DWO strategy is not required for the single condition, the proposed method is the FGAE. Table 6 shows the accuracy and F-score of each method for anomaly detection under the single condition in Case 1. The proposed method achieves optimal results in all three conditions, with accuracy and F-score of 98.80% and 99.01% under the

condition with 200 training samples, 96.84% and 97.44% under the condition with 100 training samples, 60.00% and 75.00% under the condition with 10 training samples, respectively. The DAE performs second only to the proposed method in three conditions, but the accuracy and F-score are still lower than the proposed method by 10.32% and 9.57% under the condition with 200 training samples, 9.36% and 8.81% under the condition with 100 training samples, and 4.96% and 6.71% under the condition with 10 training samples, respectively. All the methods perform relatively poor under the condition with very few training samples, as the models are prone to overfitting, resulting in the low thresholds.

Fig.13 shows the ROC curves of each method under the single condition in Case 2. The area under the curve (AUC) can indicate the anomaly detection performance with the range between 0.5 and 1. Higher AUC values represent better performance, and the AUC values for all the methods are listed in the bottom right corner in brackets. Similar to Case 1, the proposed method achieves optimal results in both conditions with AUC values of 99.81% and 99.43%, respectively. The SAE achieves the second best result under the condition of 200 training samples with the AUC value of 85.25%, which is 14.56% lower than the proposed method. The DAE achieves suboptimal results with the AUC value of 76.90% under condition of 10 training samples, which is 22.53% lower than the proposed method. The proposed method still has high AUC value under the condition with very few samples, indicating that it has potential for application in anomaly detection with few training samples, but the way of threshold determination needs to be optimized in depth.

Table 6

Evaluation metrics of the methods under the single condition in the Case 1.

Unsupervised methods	200Hz, 0N (200 training samples)		300Hz, 1000N (100 training samples)		400Hz, 1400N (10 training samples)	
	Accuracy	F-score	Accuracy	F-score	Accuracy	F-score
FGAE	**98.80±0.58**	**99.01±0.47**	**96.84±0.50**	**97.44±0.39**	**60.00±0.00**	**75.00±0.00**
MAE	88.28±0.11	89.28±0.09	86.92±0.59	88.19±0.47	54.44±1.47	68.06±0.67
VAE	88.24±0.61	89.25±0.49	84.44±1.30	86.26±0.99	55.00±1.49	67.93±0.45
DAE	88.48±0.11	89.44±0.09	87.48±0.11	88.63±0.09	55.04±0.96	68.29±0.53
SAE	87.92±0.18	88.99±0.14	84.28±1.51	86.14±1.13	50.16±0.91	66.20±0.41

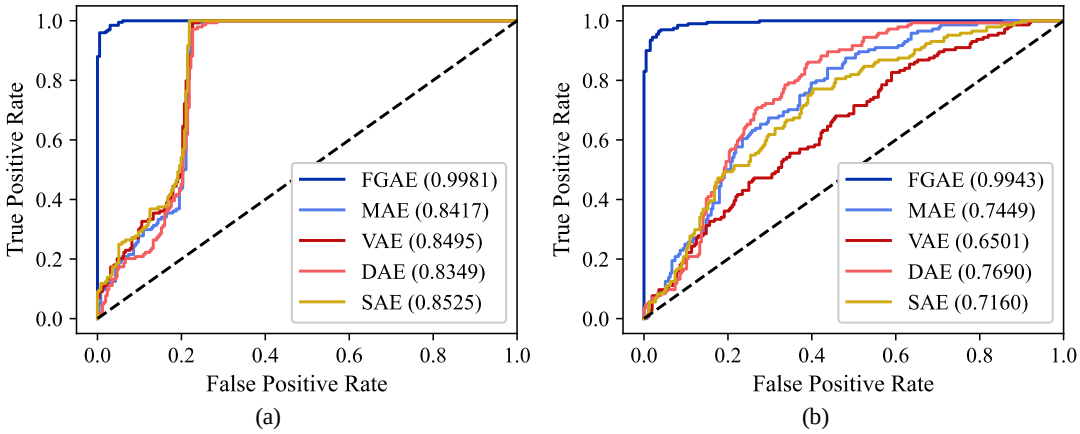

Fig.13. ROC curves for the methods under the single condition in Case 2: (a) 20Hz, 0V (200 training samples); (b) 30Hz, 2V (10 training samples).

5. Conclusions

To overcome the problems of limiting the detection task to a single operating condition and inadequate utilization of multi-channel information in machinery anomaly detection, this study proposes a new anomaly detection method named FGDAE towards complex operating conditions. The effectiveness of the proposed method is verified using two multi-condition anomaly detection tasks under the challenge of training model with multi-condition unbalanced normal data. The comparison results show: (1) The proposed method can achieve better results towards complex operating conditions compared with other popular anomaly detection methods based on autoencoder structure. (2) The developed FCG and the constructed GAAE can aggregate multi-perspective feature information among channels by establishing global structural connection between channel data from the graph structure perspective. (3) The designed DWO strategy is universal for anomaly detection methods under the challenge of training models with multi-condition unbalanced normal data. In future work, we will further explore the potential of GCN in non-Euclidean graph spaces to investigate their possibilities for anomaly detection with few training samples.

Declaration of Competing Interest

The authors declare that they have no known competing financial interests or personal relationships that could have appeared to influence the work reported in this paper.

Acknowledgements

This research is supported by the National Natural Science Foundation of China (No. 52275104) and the Natural Science Fund for Excellent Young Scholars of Hunan Province (No. 2021JJ20017).

References

[1] Chen H, Jiang B. A Review of Fault Detection and Diagnosis for the Traction System in High-Speed Trains. IEEE Transactions on Intelligent Transportation Systems, 2020, 21(2): 450-465.

[2] Xia M, Shao H, Williams D, et al. Intelligent fault diagnosis of machinery using digital twin-assisted deep transfer learning. Reliability Engineering & System Safety, 2021, 215: 107938.

[3] Kumar A, Parkash C, Vashishtha G, et al. State-space modeling and novel entropy-based health indicator for dynamic degradation monitoring of rolling element bearing. Reliability Engineering & System Safety, 2022, 221: 108356.

[4] Chen H, Jiang B, Ding S X, et al. Data-Driven Fault Diagnosis for Traction Systems in High-Speed Trains: A Survey, Challenges, and Perspectives. IEEE Transactions on Intelligent Transportation Systems, 2022, 23(3): 1700-1716.

[5] Zhou Y, Kumar A, Parkash C, et al. A novel entropy-based sparsity measure for prognosis of bearing defects and development of a sparsogram to select sensitive filtering band of an axial piston pump. Measurement, 2022, 203: 111997.

[6] Chen H, Liu Z, Alippi C, et al. Explainable Intelligent Fault Diagnosis for Nonlinear Dynamic Systems: From Unsupervised to Supervised Learning. IEEE Transactions on Neural Networks and Learning Systems, 2022, DOI 10.1109/TNNLS.2022.3201511.

[7] Zhao Z, Li T, Wu J, et al. Deep learning algorithms for rotating machinery intelligent diagnosis: An open source benchmark study. ISA transactions, 2020, 107: 224-255.

[8] Li X, Ding Q, Sun J Q. Remaining useful life estimation in prognostics using deep convolution neural networks. Reliability Engineering & System Safety, 2018, 172: 1-11.

[9] He Z, Shao H, Zhong X, et al. Ensemble transfer CNNs driven by multi-channel signals for fault diagnosis of rotating machinery cross working conditions. Knowledge-Based Systems, 2020, 207: 106396.

[10] Liu J, Pan C, Lei F, et al. Fault prediction of bearings based on LSTM and statistical process analysis. Reliability Engineering & System Safety, 2021, 214: 107646.

[11] Shi Z, Chehade A. A dual-LSTM framework combining change point detection and remaining useful life prediction. Reliability Engineering & System Safety, 2021, 205: 107257.

[12] Shao H, Jiang H, Lin Y, et al. A novel method for intelligent fault diagnosis of rolling bearings using ensemble deep auto-encoders. Mechanical Systems and Signal Processing, 2018, 102: 278-297.

[13] Yang Z, Baraldi P, Zio E. A method for fault detection in multi-component systems based on sparse

autoencoder-based deep neural networks. Reliability Engineering & System Safety, 2022, 220: 108278.

[14] Li W, Zhong X, Shao H, et al. Multi-mode data augmentation and fault diagnosis of rotating machinery using modified ACGAN designed with new framework. Advanced Engineering Informatics, 2022, 52: 101552.

[15] Chen M, Shao H, Dou H, et al. Data augmentation and intelligent fault diagnosis of planetary gearbox using ILoFGAN under extremely limited samples. IEEE Transactions on Reliability, 2022, DOI 10.1109/TR.2022.3215243.

[16] Kumar A, Vashishtha G, Gandhi C P, et al. Sparse transfer learning for identifying rotor and gear defects in the mechanical machinery. Measurement, 2021, 179: 109494.

[17] Kumar A, Gandhi C P, Zhou Y, et al. Improved CNN for the diagnosis of engine defects of 2-wheeler vehicle using wavelet synchro-squeezed transform (WSST). Knowledge-Based Systems, 2020, 208: 106453.

[18] Kumar A, Vashishtha G, Gandhi C P, et al. Tacho-less sparse CNN to detect defects in rotor-bearing systems at varying speed. Engineering Applications of Artificial Intelligence, 2021, 104: 104401.

[19] Dai J, Wang J, Huang W, et al. Machinery health monitoring based on unsupervised feature learning via generative adversarial networks. IEEE/ASME Transactions on Mechatronics, 2020, 25(5): 2252-2263.

[20] Plakias S, Boutalis Y S. A novel information processing method based on an ensemble of Auto-Encoders for unsupervised fault detection. Computers in Industry, 2022, 142: 103743.

[21] Chen Z, Li Z, Wu J, et al. Deep residual shrinkage relation network for anomaly detection of rotating machines. Journal of Manufacturing Systems, 2022, 65: 579-590.

[22] Yan H, Liu Z, Chen J, et al. Memory-augmented skip-connected autoencoder for unsupervised anomaly detection of rocket engines with multi-source fusion. ISA transactions, 2022, DOI 10.1016/j.isatra.2022.07.014.

[23] Yan S, Shao H, Xiao Y, et al. Hybrid robust convolutional autoencoder for unsupervised anomaly detection of machine tools under noises. Robotics and Computer-Integrated Manufacturing, 2023, 79: 102441.

[24] Li T, Zhou Z, Li S, et al. The emerging graph neural networks for intelligent fault diagnostics and prognostics: A guideline and a benchmark study. Mechanical Systems and Signal Processing, 2022, 168: 108653.

[25] Li T, Zhao Z, Sun C, et al. Hierarchical attention graph convolutional network to fuse multi-sensor

signals for remaining useful life prediction. Reliability Engineering & System Safety, 2021, 215: 107878.

[26] Tang Y, Zhang X, Qin G, et al. Graph Cardinality Preserved Attention Network for Fault Diagnosis of Induction Motor Under Varying Speed and Load Condition. IEEE Transactions on Industrial Informatics, 2022, 18(6): 3702-3712.

[27] Li C, Mo L, Yan R. Fault diagnosis of rolling bearing based on WHVG and GCN. IEEE Transactions on Instrumentation and Measurement, 2021, 70: 3519811.

[28] Zhao X, Jia M, Liu Z. Semisupervised Graph Convolution Deep Belief Network for Fault Diagnosis of Electormechanical System With Limited Labeled Data. IEEE Transactions on Industrial Informatics, 2021, 17(8): 5450-5460.

[29] Yang C, Liu J, Zhou K, et al. Transfer Graph-Driven Rotating Machinery Diagnosis Considering Cross-Domain Relationship Construction. IEEE/ASME Transactions on Mechatronics, 2022, 27(6): 5351-5360.

[30] Yan S, Shao H, Xiao Y, et al. Semi-supervised fault diagnosis of machinery using LPS-DGAT under speed fluctuation and extremely low labeled rates. Advanced Engineering Informatics, 2022, 53: 101648.

[31] Bruna J, Zaremba W, Szlam A, et al. Spectral networks and locally connected networks on graphs. arXiv:1312.6203, 2013.

[32] Defferrard M, Bresson X, Vanderg. heynst P. Convolutional neural networks on graphs with fast localized spectral filtering. Advances in neural information processing systems, 2016, 29.

[33] Vincent P, Larochelle H, Bengio Y, et al. Extracting and composing robust features with denoising autoencoders. Proceedings of the 25th international conference on Machine learning. 2008: 1096-1103.

[34] Kipf T N, Welling M. Variational graph auto-encoders. arXiv:1611.07308, 2016.

[35] Liu S, Johns E, Davison A J. End-to-end multi-task learning with attention. Proceedings of the IEEE/CVF conference on computer vision and pattern recognition. 2019: 1871-1880.

[36] Kingma D P, Ba J. Adam: A method for stochastic optimization. arXiv:1412.6980, 2014.

[37] Daga A P, Fasana A, Marchesiello S, et al. The Politecnico di Torino rolling bearing test rig: Description and analysis of open access data. Mechanical Systems and Signal Processing, 2019, 120: 252-273.

[38] Shao S, McAleer S, Yan R, et al. Highly accurate machine fault diagnosis using deep transfer learning.

IEEE Transactions on Industrial Informatics, 2018, 15(4): 2446-2455.

[39] Shao H, Lin J, Zhang L, et al. A novel approach of multisensory fusion to collaborative fault diagnosis in maintenance. Information Fusion, 2021, 74: 65-76.

[40] Xiao Y, Shao H, Han S Y, et al. Novel Joint Transfer Network for Unsupervised Bearing Fault Diagnosis From Simulation Domain to Experimental Domain[J]. IEEE/ASME Transactions on Mechatronics, 2022, DOI 10.1109/TMECH.2022.3177174.

[41] Gong D, Liu L, Le V, et al. Memorizing normality to detect anomaly: Memory-augmented deep autoencoder for unsupervised anomaly detection. Proceedings of the IEEE/CVF International Conference on Computer Vision. 2019: 1705-1714.

[42] Kingma D P, Welling M. Auto-encoding variational bayes. arXiv:1312.6114, 2013.

[43] Sun W, Shao S, Zhao R, et al. A sparse auto-encoder-based deep neural network approach for induction motor faults classification. Measurement, 2016, 89: 171-178.